MULTI-SCALE IMAGING AND CROSS-PROPERTY CORRELATIONS IN HETEROGENOUS SANDSTONE

Pieter W.S.K. Botha[1], Alexandra N. Golab[2], Pradeep Bhattad[2], Carley Goodwin[2], and Adrian P. Sheppard[1]

[1]The Australian National University, Canberra, Australia
[2]FEI Lithicon, Canberra, Australia

This paper was prepared for presentation at the International Symposium of the Society of Core Analysts held in Avignon, France, 8-11 September, 2014

ABSTRACT

Digital 3D image data from X-ray micro-CT (μCT), in combination with simulation software, allow for the measurement and calculation of geological and petrophysical reservoir rock properties. Similar to conventional core analysis, data obtained through digital image analysis may be used in the construction of geological models, which require upscaling for use in dynamic reservoir simulation. This paper presents some steps towards a workflow to determine core-plug scale properties through the use of reservoir characterisation data obtained from μCT imagery.

μCT enables the characterisation of geological structures in core samples over a wide range of length scales, presenting new possibilities for property prediction. A single μCT image is capable of capturing data for length scales covering approximately three orders of magnitude (μm, mm, and cm); additionally, one can acquire multiple images at different resolutions to improve data accuracy at different length scales.

In this work, 100mm tall and 25mm diameter core-plugs of heterogeneous sandstone, consisting of fine- to coarse-grained bands ranging from mm to cm in thickness, were imaged using μCT at 16μm/voxel resolution. The essential stages in the data analysis work-flow involve: 1) Plug Unitisation: automated identification of geological rock units through the analysis of grain size and ϕ logs using instantaneous rate of change, 2) Geological Characterisation: measuring the phase fractions, grain and pore size, and grain sorting of the rock units, and 3) Petrophysical Characterisation: measuring rock unit permeability and conductivity using digital simulation software. μCT Images of the 25mm diameter core-plugs have insufficient resolution to capture fine-scale features such as pore throats or clay-bound porosity; therefore, additional fine-scale data are collected in step 4) Sub-plug Imaging and Characterisation: a series of sub-plugs (typically 25mm tall x 8mm diameter) are collected from the original core-plugs, imaged at approximately 5μm/voxel resolution, and analysed in a similar way as the 25mm diameter datasets. An associated experimental program is also underway on the same samples that will link the digital core data with results from routine and special core analysis.

Results indicate linearity between grain and pore size; however, there is no clear correlation between grain size and other macro properties such as porosity and the proportion of clay minerals. Modelled permeability correlates linearly with the average pore body size after log transformation of both properties, suggesting a potential methodology for property prediction using a combination of core-plug and sub-plug scale data.

INTRODUCTION

The main research objective of this work is to identify and model correlations between geological (mineralogy, porosity, and grain and pore size), and petrophysical properties (permeability (k) and formation factor (F)) in heterogenous sandstone, by combining data at different resolutions acquired via X-ray micro-Computed Tomography (μCT). This will provide the foundation for a workflow to predict petrophysical properties from multiple sets of imaging data, ranging from high resolution data with low sampling density through to low resolution imaging with increased sample coverage but insufficient resolution and accuracy to support direct computation of petrophysical properties. The final workflow is planned to include whole-core medical CT image data on the meter scale and integration with downhole logs (not reported here).

Modern μCT core imaging, in combination with petrophysical simulation software, is fast becoming a standard tool for augmenting reservoir characterisation and modeling [1].

Due to the nature of high resolution imaging and the associated analytical equipment, whole core samples (m scale) cannot be imaged readily at the same high resolution as smaller core plugs (cm scale) or mini-plug samples (mm scale). High resolution imagery is critical to achieve reliable results for transport property simulations such as permeability, which relies on all significant pathways in the pore space being correctly represented in the image.

Limitations on sample size lead to fundamental limitations on imaging resolution. A μCT image of a 25mm diameter x 100mm tall sample, imaged using a detector with 2000 pixels per row, will have a minimum voxel size of ~13μm, which implies that rock bands with grain and pore textures smaller than ~50μm (i.e. 4 voxels across) cannot be represented with enough detail to reliably simulate petrophysical properties.

GEOLOGY AND SAMPLING

The Precipice sandstone is the early Jurassic age basal formation of the Surat Basin, in South East Queensland, Australia. Martin (1977) [2] and Whitehouse (1953) [3] provide detailed descriptions of the sedimentology and stratigraphy of the Precipice sandstone. Martin (1977) and Allen and Houston (1964) [4] describe the Precipice as a medium to coarse grained fluviatile sandstone, with low quantities of clay minerals and minor amounts of accessory minerals such as feldspar and mica. Diagenetic alterations include silica redistribution through pressure dissolution and the chemical alteration of feldspar and biotite to kaolinite.

A series of 25mm diameter x 100mm tall core plugs (25mm plugs or data) were collected from Precipice Sandstone drill core exhibiting significant heterogeneity in the form of alternating coarse- and fine-grained bands. At least one smaller 8mm diameter x 15mm

tall sub-sample (8mm plugs or data) was collected from the 25mm plugs parallel to their long axes. This paper focuses on one sample labelled PU7, taken from a depth of 1195m, containing fine- to coarse-grained bands.

WORKFLOW OVERVIEW

In the context of property prediction, the workflow relies on the availability of lower resolution images of the rock volumes of interest. The workflow steps completed for this paper are:

1. **Whole core examination and imaging:** 6m of whole core imaged at ~60µm/voxel resolution using medical-CT equipment.
2. **25mm plug selection and imaging:** plug locations are selected to cover a reasonable range of variability from fine- to coarse-grained bands. These 25mm plugs are imaged at ~16µm/voxel resolution (low resolution images).
3. **8mm plug selection and imaging:** 8mm sub-plugs cored from the 25mm samples are imaged at ~5µm/voxel resolution (high resolution). Similar to 25mm plug sampling, sub-plugging aims to capture a range of fine- and coarse-grained bands.
4. **Image unitisation:** an automated process that separates sample images into bands ("units") for individual characterisation (applied to 25mm and 8mm data).
5. **Unit characterisation:** each unit identified in step 3 above is characterised by calculating several geological properties (phase fractions, grain size and sorting, pore size and sorting) and simulating petrophysical properties (k and F). Some properties, most notably permeability, cannot be simulated accurately on the 25mm dataset, since the image resolution is not always adequate to capture pore throats.
6. **Registration and equivalent unit volume characterisation:** the 25mm dataset is registered onto the 8mm data to determine the exact location of the 8mm image in the 25mm data. The equivalent volumes in the 25mm data as those identified in the unitisation of the 8mm data are characterised for geological properties and formation factor.
7. **Cross-property correlations:** determine relationships between the calculated geological and petrophysical properties in the 8mm and 25mm datasets.
8. **Cross-resolution property correlations:** correlate geological and petrophysical properties between the 25mm and 8mm datasets.

At the moment permeability is only available for the 8mm sub-plug (~1cm^3). This current workflow is moving towards a methodology intended to predict permeability over the full volume of the 25mm plug (~60cm^3) by using correlations between permeability and geological properties (i.e. grain size, porosity, etc.) in the 25mm dataset. Two-phase flow properties such as capillary pressure, relative permeability, or resistivity index will not be considered here.

DATA COLLECTION AND ANALYSIS

µCT IMAGING AND PROCESSING

The selected core plugs were imaged in 3D using a helical scanning µCT system at The Australian National University (ANU), Canberra, Australia. Image analysis was

conducted using the Mango image analysis software and custom data processing scripts created by the authors during the course of the project.
The critical post-imaging step is that of segmentation, which maps the 16 bit grey-scale image representing X-ray attenuations to an image with a small number of discrete values or phases, where each phase represents a different material or class of material. In this study, samples were segmented, using the converging active contour method [5], into four phases: porosity (low grey-scale values); clay (intermediate values); framework minerals, mostly quartz with some feldspar; and dense minerals, including rutile and zircon. To be able to compare data from exactly the same volume in the 25mm plug as that from the 8mm sub-plug, image registration is required to align the 3D images of the 25mm and 8mm images (figure 1).

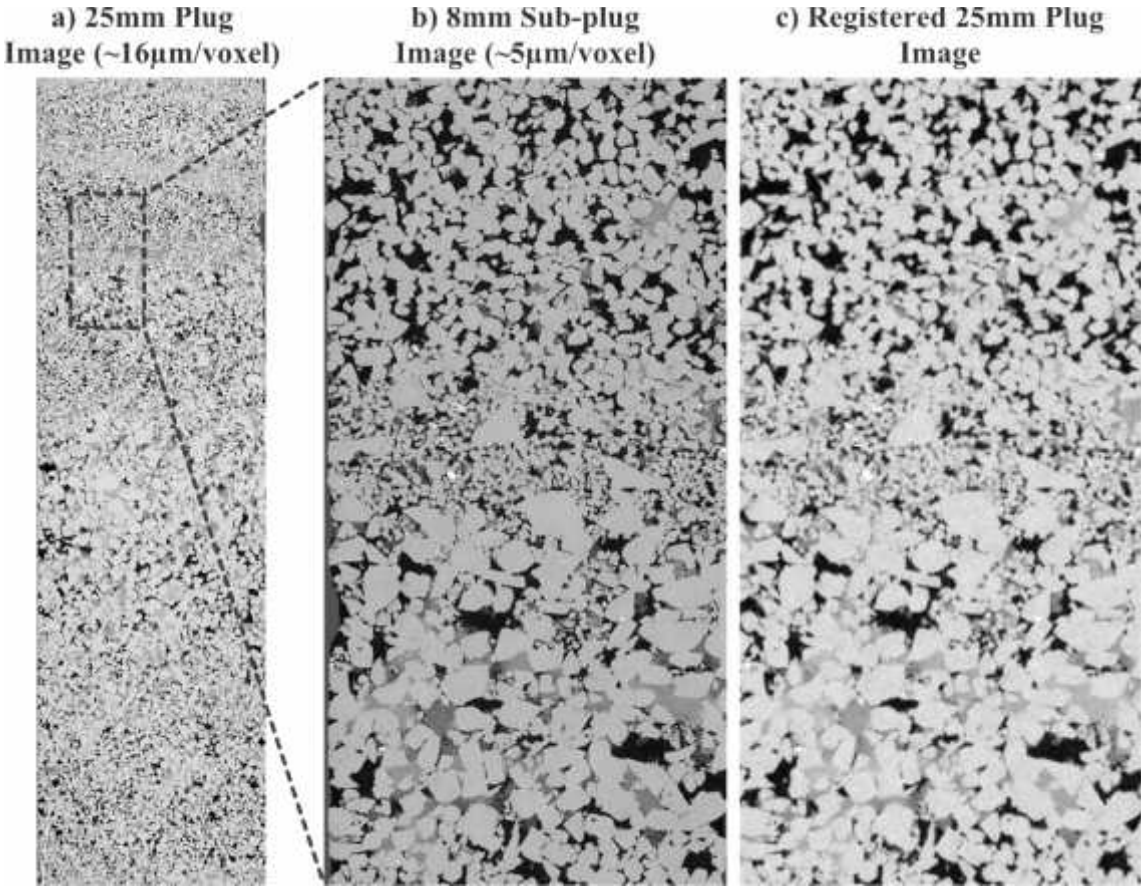

Figure 1: a) The registration process (accurate to less than one pixel) identifies the mapping to link the 8mm sub-plug image to its location within the 25mm plug, b) a magnified slice from the 8mm dataset, and c) the corresponding portion from the 25mm dataset. From this comparison it is clear how the lower resolution image contains far less information per unit volume than the 8mm dataset.

IMAGE UNITISATION

To account for sample heterogeneity a unitization procedure was developed to identify rock bands with internally consistent geological properties. Phase profiles are generated

slice-wise from the 3D segmented data file, resulting in a representation of the phase fractions resembling a wireline log, albeit at a much smaller scale. In addition, a grain size log is generated by applying a covering radius transform (CRT) [6] to the grain phase. This transform is equivalent to repeated application of morphological opening in which the structuring elements are the complete set of Euclidean balls up to the largest inscribed radius of the grain space.

Log-type data, similar to time-series data, are ideal candidates for analysis by step detection techniques. For example, in voice recognition software step detection is critical for the identification of the beginning and end of words within the audio signal [7]. Step detection analysis has also been applied to downhole well-logs by Gill (1970) [8]. Here, μCT image unitisation is achieved by analysing the gradients of the porosity and grain size (CRT) logs. For each log all local gradient maxima are identified, forming an initial division of the sample into a maximal number of units. The next step is to iteratively compare adjacent units and their properties. If the mean grain size or porosity values for two adjacent units are within a user-adjustable number of standard deviations, the boundary separating them is removed, and the routine returns to re-calculate unit properties and re-compare adjacent units. Once the routine reaches stability (no more boundaries identified for removal), the unitisation from the porosity and grain size log analyses are merged by taking boundaries from each, thus defining units in which both the grain size and porosity are considered distinct from their neighbours. The small sampling interval of one z-slice (i.e. the height of one voxel) in combination with high but non-uniform levels of high-frequency fluctuations in the logs, requires a smoothing operation before the gradient-based analysis can be performed. Conventional time series data such as weather or financial data can be smoothed using a rolling average with constant window size, however, given that the μCT log data are generated from rock volumes with spatially varying properties, and to prevent over or under smoothing, a dynamic window size is calculated based on grain size. For each z-slice the averaging range is given by the average grain size from the CRT analysis. The non-uniform smoothing implemented here is based on the hypothesis that to achieve a representative average for any given z-slice, the averaging window must be small enough so that the data does not contain sharp fluctuations resulting from individual grain CRT values. Gradient logs are smoothed using a constant averaging range because it is a consistent measure of instantaneous rate of change. The non-uniform smoothing determined from grain CRT values is applied also to the porosity log.

UNIT CHARACTERISATION

Each rock unit identified in the unitisation procedure is characterised by calculating its geological and petrophysical properties. To improve the statistics to be used later during property correlations, each unit is characterised individually and divided into multiple sub-volumes. The top and bottom slices of the sub-volumes are chosen to align with the boundaries from the unitisation procedure. The sizes of the sub-volumes are determined as a function of the grain size in such a way so that each sub-volume approximates a representative element volume for accurate and statistically relevant data. Petrophysical

properties and phase fractions are determined simultaneously on the same sub-volumes chosen for geological characterisation.

CALCULATING GRAIN AND PORE SIZE AND SORTING

Grain and pore size and sorting provide quantitative data for the analysis and interpretation of sedimentary processes and environments [9]. Assuming a log-normal size distribution, sediment grain and pore sorting are measures of spread of the distribution curves [10]. Sorting is generally negatively correlated with porosity and permeability, following that porosity is grain size independent for two rock volumes with equal sorting and grain packing [11]. To calculate grain and pore size and sorting, the μCT analysis software compiles volume-weighted size distribution data for grains and pores expressed in number of voxels. The size classes are converted to equivalent sphere diameter (ESD) [12]. Following the assumption that the ESD is distributed according to a log-normal distribution, one computes the so-called phi units as the negative logarithm of the ESD values [13]. A cumulative logarithmic ESD size distribution curve and a linear cumulative phi-scale distribution curve are used to determine the median in μm and phi units. Grain and pore sorting are calculated from the 5th, 16th, 84th, and 95th percentiles of these distributions using the standard equation from Folk and Ward (1957) [10].

PETROPHYSICAL SIMULATIONS AND PHASE FRACTIONS

Petrophysical simulations of absolute permeability (k) and formation factor (F) were performed using the Morphy software suite [14,15]. Permeability is calculated using the D3Q19 (3 dimensional lattice with 19 possible momenta components) Lattice-Boltzmann method [16]. The fluid, which is represented by a series of particles during the simulation, is placed under a pressure gradient by a body force [17,18]. The formation factor is calculated by solving Laplace's equation using a finite element formulation to solve the potential field in a homogenous electrical field of unity strength [14,19].

RESULTS AND DISCUSSION

UNITISATION

The unitisation results include phase fraction logs, grain and pore size logs, the absolute gradients of the ϕ and grain size logs, and the resulting unitisation of the 25mm and 8mm data for sample PU7 alongside a 2D image slice for each sample (figure 2a and b). The 25mm and 8mm images are subdivided into 18 and 3 units respectively.

PROPERTY CROSS-CORRELATIONS

Both the 25mm and 8mm datasets show negative correlation between ϕ and clay fraction, supporting the descriptions of Martin (1977) [2] that most of the clay was formed through diagenetic processes (figure 3a and b). Grain sizes calculated from the 8mm and 25mm datasets show strong clustering according to the unitisation, along with a linear relationship between those clusters (figure 4a), while pore sizes from these two

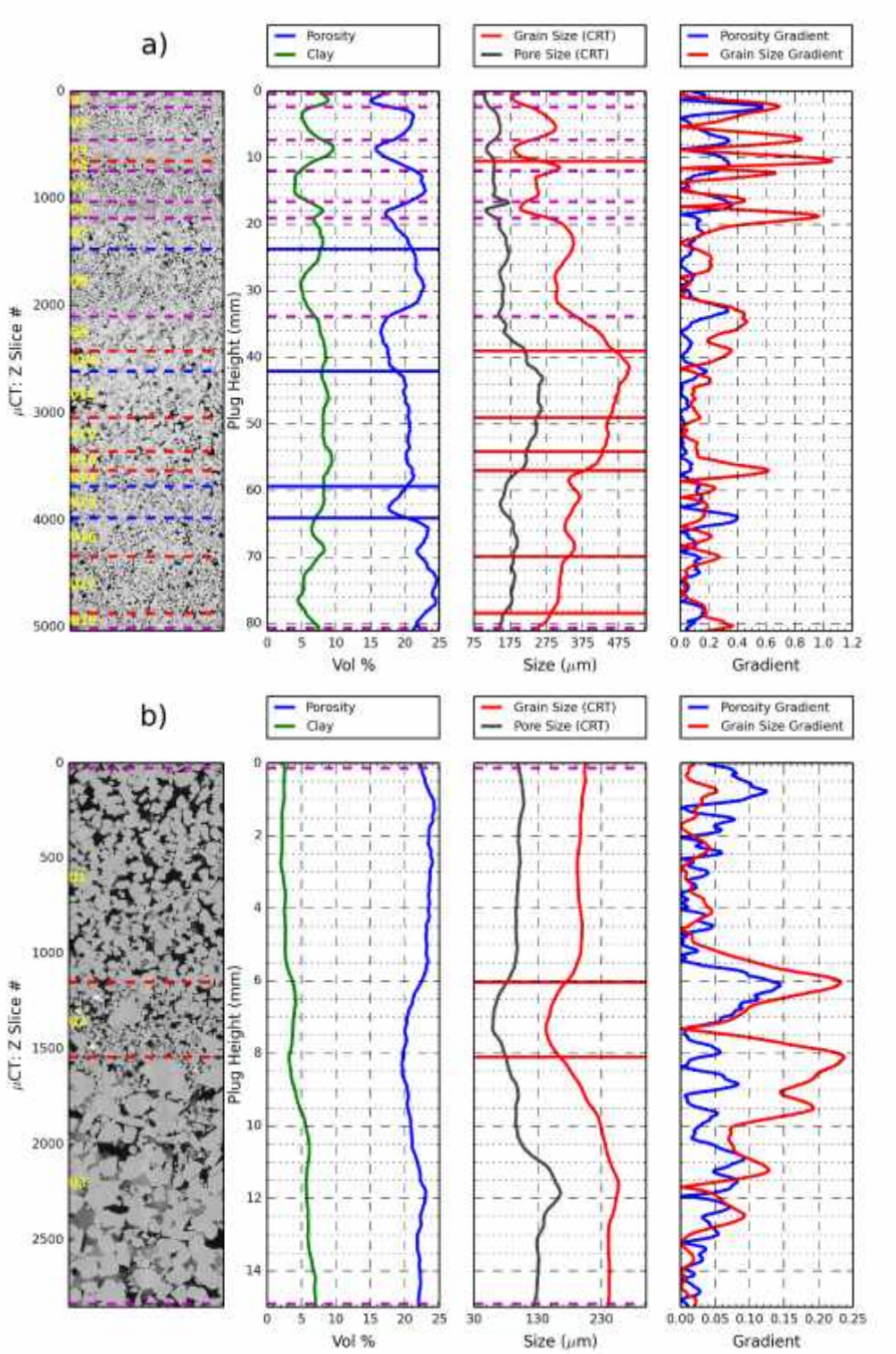

Figure 2: a) 25mm plug image unitisation, and b) 8mm sub-plug image unitisation. Horizontal blue lines indicate boundaries from the ϕ log, horizontal red lines indicate boundaries from the grain size log, and horizontal stippled magenta lines indicate boundaries identified in both the grain size and ϕ logs.

datasets show little clustering, but still strong linear correlation (figure 4b), supporting image unitisation based on grain size. Figure 4 shows that the 25mm image slightly over-estimates grain and pore sizes relative to the 8mm data, which is attributed to the fact that the 8mm image naturally captures finer scale features, resulting in a higher proportion of small pores, and therefore a slightly lower median pore size.

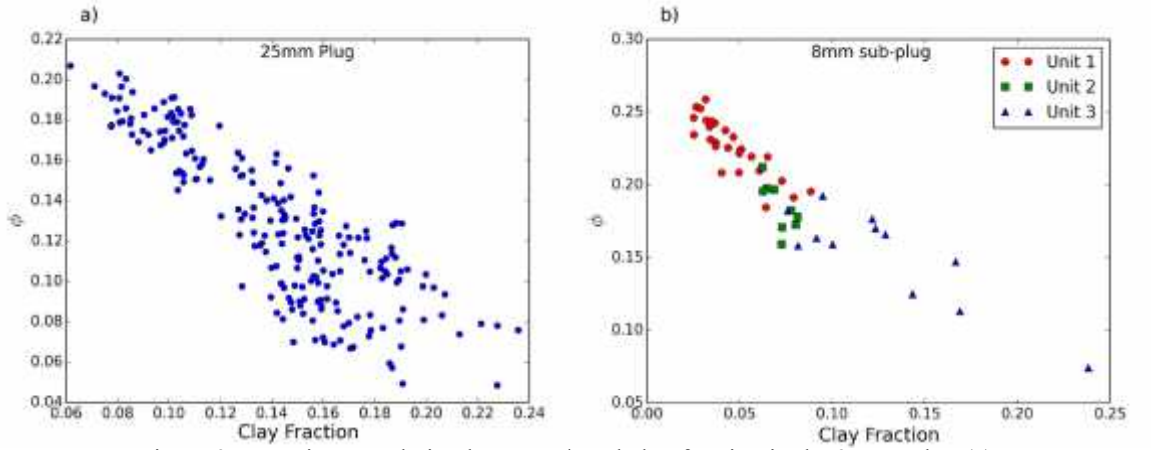

Figure 3: Negative correlation between ϕ and clay fraction in the 25mm plug (a), and in the 8mm sub-plug (b).

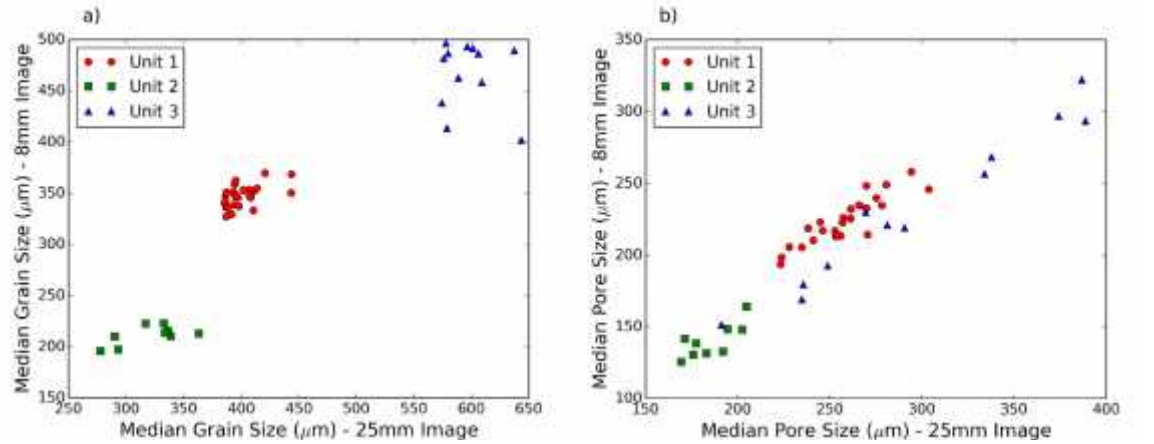

Figure 4: a) Low- and high-resolution data for grain size (Equivalent Spherical Diameter, ESD) show clustering according to the unitisation, (b) pore sizes (ESD) from the low- and high-resolution images demonstrate less clustering. In both cases the data exhibit a general linear relationship.

Initial investigation of the 25mm data showed that direct simulation of k is highly inaccurate since this lower resolution image fails to capture many pore throats as open porosity, thereby preventing the porosity phase from percolating. These throats are, however, frequently classified as intermediate (clay) phase. The permeability solver allows for fractional k to be set for each phase, therefore, in an attempt to gather some k data from the 25mm plug image, a k simulation was conducted by assigning a fractional k of 0.25 to the intermediate (clay) phase (ϕ is set to 1 – completely permeable). The

resulting k values are not accurate in themselves, but show a strong correlation with pore size on a log-log plot, and may correlate better with the true permeability in the lower resolution images.

Log(k) (simulated using the 8mm sub-plug image) shows positive correlation with ϕ from the 8mm and equivalent volume 25mm data (figure 5a and b), which is consistent with results from previous investigators [13]. Log(k) from the 8mm sub-plug image shows negative correlation with grain sorting in both the 8mm and equivalent volume 25mm data (figure 6a and b). The over-estimated pore size in the 25mm image (figure 4b) may raise an expectation that porosity would also be over-estimated, and that permeability would be higher in the 25mm image than in the 8mm data; however, the lower voxel density in the 25mm image affects all phases equally, resulting in similar porosities from the 25mm and 8mm data; additionally, the lack of pore throats imaged in the 25mm data dominates the permeability simulation, resulting in lower permeability for the 25mm image.

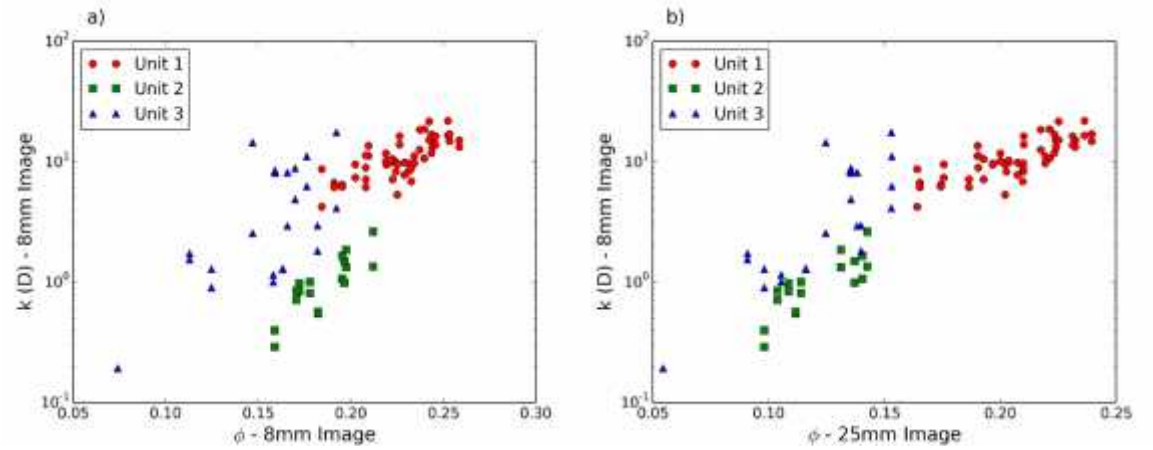

Figure 5: a) Positive correlation between log(k) and ϕ in the 8mm sub-plug, and b) positive correlation between log(k) (from the 8mm sub-plug) and ϕ in the equivalent volume 25mm data.

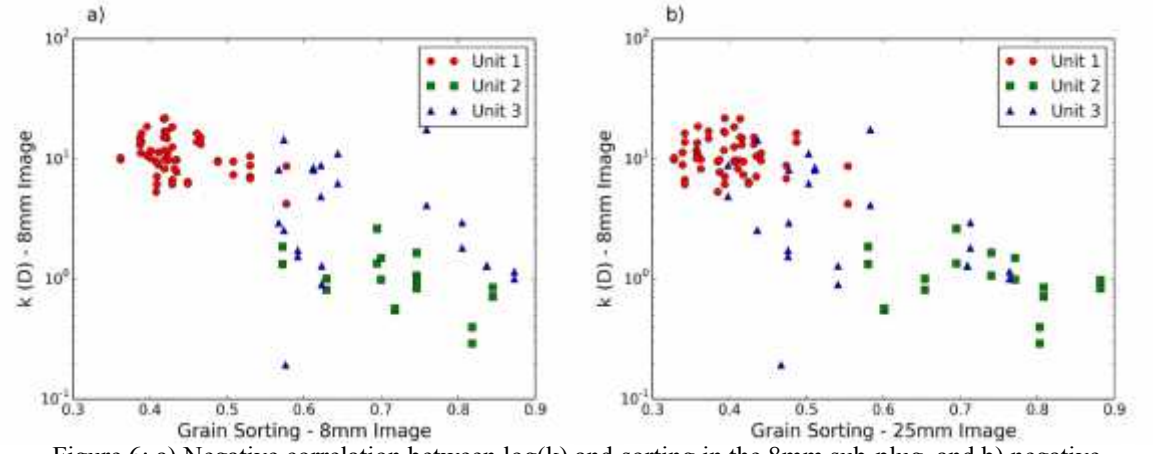

Figure 6: a) Negative correlation between log(k) and sorting in the 8mm sub-plug, and b) negative correlation between log(k) (from the 8mm sub-plug) and sorting in the equivalent volume 25mm data.

The sampling location is a particularly permeable portion of the Precipice sandstone, with some simulated values above the maximum value of nearly 8 Darcies reported by Bradshaw et al. (2009) [20]. The simulated values are not unexpected as very coarse open sandstones with grain sizes above 1mm can be expected to have permeabilities well in excess of 10 Darcies. Further verification of simulated permeability values through experimental analysis is currently under way.

As expected for relatively clean sandstone, log(F) correlates well with ϕ within each of the three units in both the 8mm and equivalent volume 25mm data (figure 7a and b). Similar to the permeability solver, fractional conductivity can be set for each phase during formation factor simulation. Standard formation factor simulation procedures assign conductivity to the clay phase based on clay-bound porosity and an assumed cementation exponent. Because of the partial volume effect, the volume around pore throats are often classified as intermediate (clay) phase. Since this phase is conductive, the formation factor calculated from the lower resolution 25mm image is similar to that from the 8mm data.

After simulation the cementation exponent is calculated as the slope of the best fit line based on robust linear modeling, which uses an iteratively re-weighted least squares method with a robust criterion estimator to estimate a robust linear model to minimise outlier influence [21]. It might be argued that calculating cementation exponent on a relatively small number of data points may not be sufficiently accurate, however, the data show some variability in the cementation exponent, thereby supporting unit-specific characterisation. Log(k) from the 8mm sub-plug image shows excellent linear correlation with log(F) in the 8mm and equivalent volume 25mm plug data (figure 8a and b). Cross-property correlations between permeability, simulated using high-resolution images, and fundamental geological properties (porosity and grain sorting) and formation factor simulations using low-resolution images, provide encouraging evidence supporting cross-resolution predictions of petrophysical properties (figures 5b, 6b, 7b).

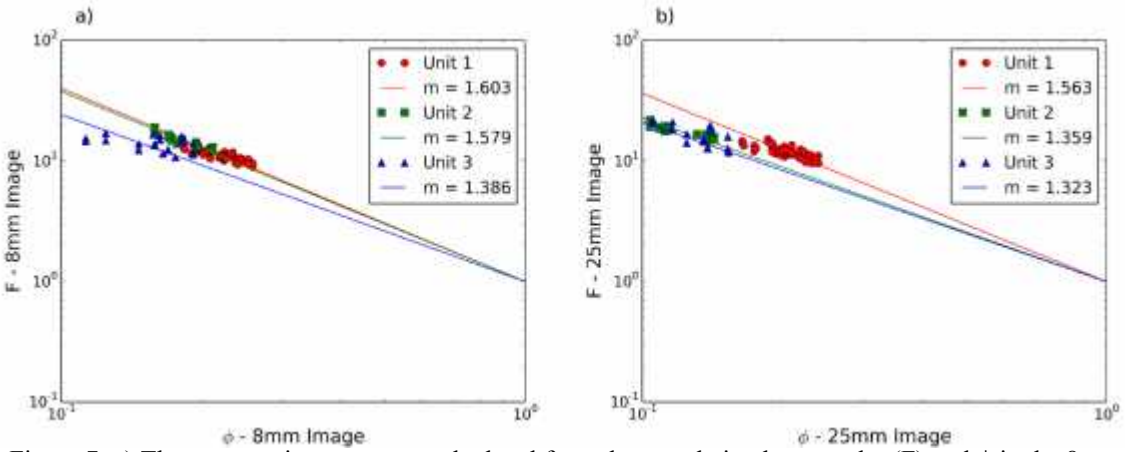

Figure 7: a) The cementation exponent calculated from the correlation between log(F) and ϕ in the 8mm sub-plug, and b) from correlation between log(F) and ϕ in the equivalent volume 25mm data.

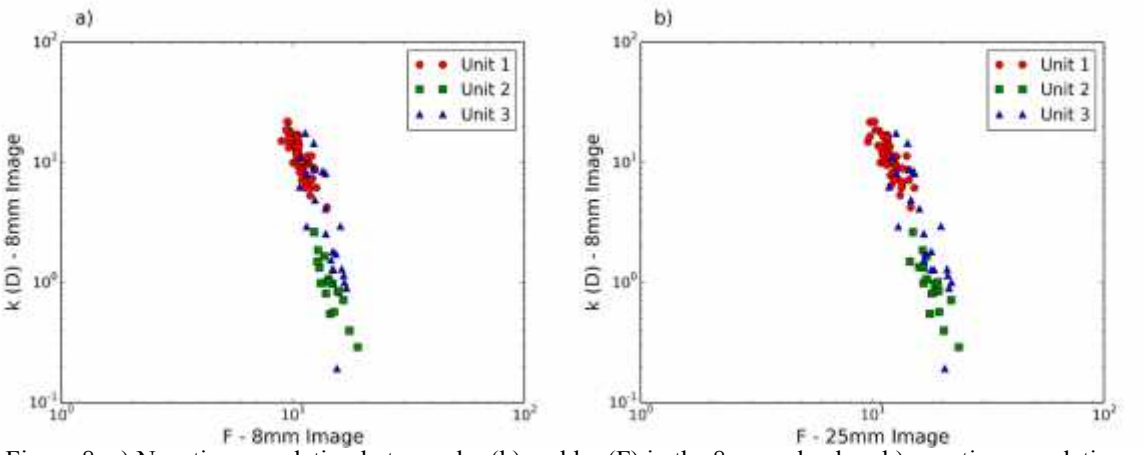

Figure 8: a) Negative correlation between log(k) and log(F) in the 8mm sub-plug, b) negative correlation between log(k) (from the 8mm sub-plug) and log(F) in the equivalent volume 25mm data.

CONCLUSION AND FUTURE WORK

The results presented here suggest that multi-scale μCT imaging of core plugs, and the systematic geological and petrophysical characterisation of plug volumes using guidelines from a unitisation process, can produce cross-resolution property correlations to enable predictions of petrophysical properties where such properties could not be measured directly.

More work is needed to complete the property prediction workflow. Areas of focus include developing statistical models to propagate the correlation results to the whole 25mm dataset, and testing the workflow on other similar samples, while future research will investigate techniques of integrating μCT data with downhole log data as a potential method for predicting properties at core and well-bore scale.

ACKNOWLEDGEMENTS

The authors wish to acknowledge financial assistance provided through Australian National Low Emissions Coal Research and Development (ANLEC R&D). ANLEC R&D is supported by Australian Coal Association Low Emissions Technology Limited and the Australian Government through the Clean Energy Initiative. Pieter Botha acknowledges the Australian Department of Education for the support of an APA. Adrian Sheppard acknowledges the ARC for support of a future fellowship. High Performance Computing resources were provided by the Australian National Computing Infrastructure (NCI).

REFERENCES

1. Cnudde V., Boone M.N., "High-resolution X-ray computed tomography in geosciences: a review of the current technology and applications," *Earth Science Reviews,* (2013) 123, 1-17.
2. Martin K. R., "Sedimentology of the Precipice Sandstone, Surat Basin, Queensland." *PhD Thesis, University of Queensland*, (1977).
3. Whitehouse F.W., "The mesozoic environments of Queensland," *Aust. N.Z. Ass. Adv. Sci. Rep., (1953)* 29, 83-106.

4. Allen R.J. and Houston B.R., Petrology of Mesozoic sandstones of Carvarvon Highway section, western Bowen and Surat Basins," *Geological Survey of Queensland Rep .6*, (1964)
5. Sheppard A.P., Sok R., and Averdunk H., "Techniques for image enhancement and segmentation of tomographic images of porus materials", *Physica A: Statistical mechanics and its applications*, (2004) 339,145-151.
6. Hazlett R., "Simulation of capillary-dominated displacements in microtomographic images of reservoir rocks," *Transp. Porous Media, (1995)* 20, 21-35.
7. Li Q., Zheng J., Tsai A., and Zhou Q.*,"*Robust endpoint detection and energy normalization for real-time speech and speaker recognition," *IEEE Transactions of Speech and Audio Processing*, (2002) 10, No. 3.
8. Gill D, "Application of a statistical zonation method to reservoir evaluation and digitized-log analysis," *AAPG Bulletin*, (1970) 54, Issue 5, 719-729.
9. Visher G., "Grain size distribution and depositional processes," *Journal of Sedimentary Petrology*, (1969) 39, No. 3, 1074-1106.
10. Folk R.L. and Ward W.C., "Brazos River Bar: a study in the significance of grain size parameters," *Journal of Sedimentary Petrology, (1957)* 27, No. 1, 3-26.
11. Nelson P.H., "Permeability-porosity relationships in sedimentary rocks," *The Log Analyst*, (1994), May-June, 38-62.
12. Jennings B.R. and Parslow K., "Particle size measurement: the equivalent spherical diameter," *Proc. R. Soc. Lond. A*, (1988) 419, 137-149.
13. Krumbein W.C., "Size frequency distributions of sediments," *Journal of Sedimentary Petrology*, (1934) 4, 65–77.
14. Arns C.H., Knackstedt M.A., Pinczewski W.V., and Lindquist W.B., "Accurate estimation of transport properties from microtomographic images," *Geophys. Res. Lett.*, (2001) 28, No. 17, 3361–3364.
15. Arns C.H., Knackstedt M.A., Pinczewski W.V., and Martys M.S., "Virtual permeametry on microtomographic images," *J. Pet. Sci Eng.* (2004) 45, 41-46.
16. Qian Y.-H. and Zhou Y., "Complete Galilean-invariant lattice BGK models for the Navier-Stokes equation," *Europhys. Lett.*, (1998) 42, No.4, 359–364.
17. Ferreol B. and Rothman D.H., "Lattice-Boltzmann simulations of flow through Fontainebleau sand- stone," *Transport in Porous Media*, (1995) 20, 3–20. .
18. Martys N.S. and Chen H., "Simulation of multicomponent fluids in complex three-dimensional geometries by the lattice Boltzmann method," *Phys. Rev. E*, (1996) 53, No. 1, 743–750.
19. Arns C.H., Knackstedt M.A., Pinczewski W.V., and Garboczi E.G., "Computation of linear elastic properties from microtomographic images: Methodology and agreement between theory and experiment," *Geophysics*, (2002) 67, No. 5, 1396–1405.
20. Bradshaw B.E., Spencer L.K., Lahtinen, A.C., Khider K., Ryan D.J., Colwell J.B., Chirinos A., and Bradshaw J., "Queensland carbon dioxide geological storage atlas" (2009).
21. Huber P.J, "Robust Statistics (2nd ed.)," *Hoboken, NJ: John Wiley & Sons Inc*, (2009).